

Study of the daily and seasonal atmospheric CH₄ mixing ratio variability in a rural Spanish region using ²²²Rn tracer

Claudia Grossi^{a,1,2}, Felix R. Vogel^b, Roger Curcoll^{a,3}, Alba Àgueda^{a,4}, Arturo Vargas^c, Xavier Rodó^{a,d,3,5}
Josep-Anton Morguí^{a,e,3}

5

^a Institut Català de Ciències del Clima (IC3), Barcelona, Spain

^b Climate Research Division, Environment and Climate Change Canada, Toronto, Canada

^c Institut de Tècniques Energètiques (INTE), Universitat Politècnica de Catalunya (UPC), Barcelona, Spain

10 ^d Institució Catalana de Recerca i Estudis Avançats (ICREA), Barcelona, Spain

^e Departament Biologia Evolutiva, Ecologia i Ciències Ambientals, Universitat de Barcelona (UB), Barcelona, Spain

Present addresses:

¹ Institut de Tècniques Energètiques (INTE), Universitat Politècnica de Catalunya (UPC), Barcelona, Spain

15

² Physics Department, Universitat Politècnica de Catalunya (UPC), Barcelona, Spain

³ Institut de Ciència i Tecnologia Ambientals (ICTA), Universitat Autònoma de Barcelona (UAB), Cerdanyola del Vallès, Spain

⁴ Centre d'Estudis del Risc Tecnològic, Universitat Politècnica de Catalunya (UPC) - BarcelonaTech, Barcelona, Spain

20

⁵ CLIMA2, Climate and Health Program, ISGlobal (Barcelona Institute of Global Health), Barcelona, Spain

Correspondence to: Claudia Grossi (claudia.grossi@upc.edu), Felix Vogel (felix.vogel@canada.ca)

Abstract. The ClimaDat station at Gredos (GIC3) has been continuously measuring atmospheric (dry air) mixing ratios of carbon dioxide (CO₂) and methane (CH₄), as well as meteorological parameters, since November 2012. In this study we investigate the atmospheric variability of CH₄ mixing ratios between 2013 and 2015 at GIC3 with the help of co-located observations of ²²²Rn concentrations, modelled ²²²Rn fluxes and modelled planetary boundary layer heights (PBLH). Both daily and seasonal changes in atmospheric CH₄ can be better understood with the help of atmospheric concentrations of ²²²Rn (and the corresponding fluxes). On a daily timescale, the variation in the PBLH is the main driver for ²²²Rn and CH₄ variability while, on monthly timescales, their atmospheric variability seems to depend on emission changes. To understand (changing) CH₄ emissions, nocturnal fluxes of CH₄ were estimated using two methods: the Radon Tracer Method (RTM) and a method based on the EDGARv4.2 bottom-up emission inventory using FLEXPARTv9.0.2 footprints. The mean value of RTM-based methane fluxes (FR_CH₄) is 0.11 mg CH₄ m⁻² h⁻¹ with a standard deviation of 0.09 mg CH₄ m⁻² h⁻¹ or 0.29 mg CH₄ m⁻² h⁻¹ with a standard deviation of 0.23 mg CH₄ m⁻² h⁻¹ when using a rescaled ²²²Rn map (FR_CH₄_rescale). For

35

our observational period, the mean value of methane fluxes based on the bottom-up inventory (FE_CH₄) is 0.33 mg CH₄ m⁻² h⁻¹ with a standard deviation of 0.08 mg CH₄ m⁻² h⁻¹. Monthly CH₄ fluxes based on RTM (both FR_CH₄ and FR_CH₄_rescale) show a seasonality which is not observed for monthly FE_CH₄ fluxes. During January-May, RTM-based CH₄ fluxes present mean values 25% lower than during June-December. This seasonal increase of methane fluxes calculated by RTM for the GIC3 area appears to coincide with the arrival of transhumant livestock at GIC3 in the second semester of the year.

Keywords: methane, flux, radon, atmosphere, livestock, EDGAR, FLEXPART.

45 **Introduction**

The impact of the atmospheric increase of greenhouse gases (GHGs) on climate change is well known (IPCC, 2013). GHGs emissions, due to natural as well as anthropogenic sources, are currently estimated and reported by each national agency to the United Nations Framework Convention on Climate Change (UNFCCC). A better understanding of the underlying processes causing these emissions can help in the implementation of future emission reduction strategies. Methane (CH₄) is the second most important anthropogenic GHG that is covered by the UNFCCC. The atmospheric mixing ratio of CH₄ has substantially changed since pre-industrial times from a global average of 715 nmol mol⁻¹ to more than 1774 nmol mol⁻¹ (IPCC, 2013). Nowadays, the contribution of CH₄ related to anthropogenic activities in the atmosphere represents about 25% of total additional anthropogenic radiative forcing (IPCC, 2013). However, CH₄ has a relatively short lifetime in the atmosphere (~ 9 years) and this makes it relevant in defining immediate and efficient emission reduction strategies (Prinn et al., 2000). Particularly in Spain, man-made methane emissions are mainly due to enteric fermentation (38%), management of manure (20%), and landfills (36%) (WWF, 2014; MMA, 2016). The remaining methane contributions in Spain are due to rice cultivation (e.g. Àgueda et al., 2017), coal mining, leaks in natural gas infrastructures and waste water treatment. The CH₄ emission due to enteric fermentation related to livestock is directly linked to the number of animals of each type/breed of cattle, their age, their diet and environmental conditions (MMA, 2016). Spanish CH₄ emissions due to enteric fermentation were estimated to be 11,704 Gg CO₂-^{eq} (MMA, 2016).

65 In order to estimate GHGs emissions, bottom-up (based on fuel consumption and anthropogenic activity data) and top-down methods (based on atmospheric observations and modelling) are both widely applied and the scientific community has focussed on reducing their related uncertainties and understanding systematic inconsistencies (e.g. Vermeulen et al., 2006; Bergamaschi et al., 2010; NRC, 2010; Jeong et al., 2013; Hiller et al., 2014). Top-down methods usually require both high-quality and long-term GHGs observations. European projects, such as InGOS (www.ingos-infrastructure.eu), and infrastructures, such as ICOS (www.icos-infrastructure.eu), aim to offer atmospheric CO₂ and non-CO₂ GHGs data and data products to better understand GHGs fluxes in Europe and adjacent regions.

Unfortunately, in some European regions, such as Spain, there is still a significant lack of high-quality atmospheric GHGs observations. The Catalan Institute of Climate Sciences (IC3) has been working since 2010 within the ClimaDat project in setting up a network of stations in national parks for continuous measurements of mixing ratios of GHGs, tracers and meteorological parameters (www.climadat.es). The IC3 network mainly aims to monitor and study the exchange of GHGs between the land surface and the lower atmosphere (troposphere) in different ecosystems, which are characterized by different biogenic and anthropogenic processes, under different synoptic conditions.

Besides GHGs mixing ratios, co-located observations of additional gases can provide us with useful tracers for source apportionment studies or to help us to better understand atmospheric processes (e.g. Zahorowski et al., 2004). The radioactive noble gas radon (^{222}Rn), due to its chemical and physical characteristic (e.g. Nazaroff and Nero, 1988), is being extensively used for studying atmosphere dynamics, such as boundary layer evolution (e.g. Galmarini, 2006, Vinuesa and Galmarini, 2007), and soil-atmosphere exchanges (e.g. Schery et al., 1998; Zahorowski et al., 2004; Szegvary et al., 2009; Grossi et al., 2012; Vargass et al., 2015; Grossi et al., 2016). European GHGs monitoring infrastructures already include atmospheric ^{222}Rn monitors in their stations (e.g. Arnold et al., 2010; Zimnoch et al., 2014; Schmithüsen et al., 2016). The co-evolution of atmospheric ^{222}Rn and GHGs concentrations can also be used within the Radon Tracer Method (RTM) to estimate local/regional GHGs fluxes (e.g. Van der Laan et al., 2010; Levin et al. 2011; Vogel et al. 2012; Wada et al., 2013; Grossi et al., 2014).

In this study we analysed the time series of atmospheric CH_4 mixing ratios measured at the IC3 station in Gredos and Iruelas (GIC3) between January 2013 and December 2015. The main aim was to investigate the main drivers that influence the daily and seasonal variability of methane concentrations in this mountainous rural southern European region. The GIC3 station is located on the Spanish plateau, an area mainly characterized by livestock activity and where transhumance is still practiced (Ruiz Perez and Valero Sáez, 1990). This is an ancestral activity consisting of the seasonal movement of livestock over long distances to reach warmer regions during the winter together with a return to the mountains in summer where pastures are greener and more suitable for grazing activities (Ruiz Perez and Valero Sáez, 1990; López Sáez et al., 2009). The livestock leaves the GIC3 region to go to southern Spanish regions during the cold period. The enteric fermentation due to digestive processes in animals could thus be a significant CH_4 source in this area. The Unión de Pequeños Agricultores (UPA, 2009) reports that between 2004 and 2009 an average of 800,000 transhumant animals were hosted in Spain and 40,000 (5% of total) were counted in the province of Ávila (extension: 8,048 km^2), where the GIC3 station is located. According to the available literature, in this area 85% of livestock still performs transhumance, with 500 stockbreeders moving every winter from the Gredos Natural Park (GNP) to warmer areas of Spain, such as Extremadura (Ruiz Perez and Valero Sáez, 1990; López Sáez et al., 2009; Libro Blanco, 2013). Generally, this mobility of cattle and associated CH_4 emissions (i.e. a major regional CH_4 source) cannot easily be included in country-wide (annual) inventories because it has not yet been properly quantified and reported by nations. The present study aims to highlight the utility of ^{222}Rn as a tracer to retrieve independent GHGs fluxes on a monthly basis using atmospheric ^{222}Rn and CH_4 data. This work represents a first step towards a better characterization of transient sources, such as transhumant livestock

for CH₄, which could help to improve national emissions inventories. Finally, it offers new CH₄ data for
115 an under-sampled area which will help in the improvement of the regional and global methane budgets.

GIC3 is a new atmospheric station so its location, the surrounding region and the instrumentation used at
this station are described in the methodology section of this manuscript. In the first part of the results
section both the daily and seasonal changes in CH₄ mixing ratios observed at the GIC3 station have been
120 analysed in relation to ²²²Rn and PBLH variability. In the second part, the nocturnal CH₄ fluxes and their
monthly variability have been estimated by the Radon Tracer Method (RTM), following Vogel et al.
(2012), and using an emission inventory for CH₄ (EDGARv4.2). Both flux estimation methods have been
applied using the same source region as modelled by the atmospheric transport model FLEXPARTv9.0.2.
The possible influence of large cities surrounding GIC3 and of seasonally changing meteorological
125 conditions on the retrieved CH₄ fluxes has also been investigated. Finally, the difference in CH₄ fluxes
between the Cattle season, when livestock is present in the GIC3 region, and the No-Cattle season, when
the transhumant cattle have migrated to the south of Spain, calculated using the RTM, has been estimated.

2 Methods

2.1 Study site: Gredos and Iruelas station (GIC3)

130

The Gredos and Iruelas station (GIC3) is located in a rural region of the Spanish central plateau (40.35°N;
5.17°E; 1440 m above sea level (a.s.l.)), as shown in Figure S1 of the supplement. GIC3 is located on the
west side of the Gredos National Park (GNP), which has a total extension of 86,397 ha. The mountains of
the GNP form the highest mountain range in the E-W orientated central mountain system. The GNP has a,
135 predominantly, granitic basement and is thus covered by soil with high activity levels of ²²⁸U (Nazaroff
and Nero, 1988). The average ²²²Rn flux in this area is about 70-100 Bq m⁻² h⁻¹ (e.g. López-Coto et al.,
2013; Karstens et al., 2015), which is almost twice the average radon flux in central Europe (Szegvary et
al., 2009, López-Coto et al., 2013; Grossi et al., 2016). The vegetation in the GIC3 area is stratified
according to altitude and the main land use practice is a mixture of agro-forestry exploitation (EEA, 2013)

140

Livestock farming is one of the main economic activities in the area around the GIC3 station (Ruiz Perez
and Valero Sáez, 1990; López Saéz et al., 2009; MMA, 2016; Hernández, 2016). In the GNP the seasonal
migration of livestock starts between November and December, when they travel to the south of the
Iberian Peninsula, and they do not return until late May-mid June (Ruiz Perez and Valero Sáez, 1990). In
145 Figure S2 of the supplement, a map of the main Spanish transhumant paths is presented. Unfortunately,
no specific reports of cattle mobility data are so far available for the GIC3 area.

Besides livestock activities, there are three small-sized to medium-sized water reservoirs and four
medium-sized to large cities in the wider area surrounding GIC3. The water reservoirs as well as several
150 activities present in the cities, e.g. landfills or waste water treatment plants, represent CH₄ sources which
could also influence methane concentrations observed at the GIC3 station under specific synoptic

conditions. The water reservoirs are located in the west and north-west area of GIC3: i) The Gabriel and Galan reservoir with an extension of 4683 ha (40.25° N; -6.13° E; 80 km away from GIC3); (ii) Santa Teresa with an extension of 2663 ha (40.60° N; -5.58° E; 42 km away from GIC3); (iii) Almendra with an extension of 7940 ha (41.25° N; -6.26° E; 120 km away from GIC3). The metropolitan area of Madrid, which comprises about 6.3 million inhabitants, is situated approximately 120 km to the east of GIC3. Valladolid, located 150 km to the west of GIC3, is reported to have approximately 416,000 inhabitants, while smaller cities like Salamanca (84 km to the north-west) and Ávila (55 km to the north-east) only have 229,000 and 59,000 inhabitants, respectively. More information about these four cities is reported in Table S1 of the supplement.

2.2 Atmospheric measurements of CH₄ and ²²²Rn

2.2.1 Air sampling

Atmospheric CH₄, CO₂ and ²²²Rn concentrations have been continuously measured since November 2012 at the GIC3 station (air inlet 20 m above ground level (a.g.l.) tower). CH₄ and CO₂ are measured with a frequency of 0.2 Hz using a G2301 analyzer (Picarro Inc., USA). Hourly atmospheric ²²²Rn concentrations are measured using an Atmospheric Radon MONitor (ARMON) (Grossi et al., 2012; Grossi et al., 2016). A schematic diagram of the measurement set-up used at the GIC3 station is shown in Figure S3 of the supplement.

The Picarro Inc. G2301 analyzer is calibrated every two weeks using 4 secondary working gas standards, which are calibrated at the beginning and end of their lifetime against seven standards of the National Oceanic and Atmospheric Administration (NOAA) (calibration scales are WMO-CO₂-X2007 and WMO-CH₄-X2004 for CO₂ and CH₄, respectively). A target gas is analyzed daily for 20 minutes in order to check the stability and quality of the instrument calibration. For the length of the study, the instrument repeatability for CH₄ was 0.80 nmol mol⁻¹, the long term reproducibility was 0.36 nmol mol⁻¹ and the observe bias was 0.81 nmol mol⁻¹. Previous values were calculated according to the definitions of the World Meteorological Organization (WMO, 2009). The ARMON instrument was installed at the GIC3 station in collaboration with the Institute of Energetic Techniques of the Universitat Politècnica de Catalunya (INTE-UPC). The ARMON is a self-designed instrument based on α spectrometry of ²¹⁸Po, collected electrostatically on a passive implanted detector. The monitor has a minimum detectable activity of 150 mBq m⁻³ (Grossi et al., 2012). The performance of the ARMON was previously tested against a widely used ²²²Rn progeny monitor and good results were observed (Grossi et al., 2016).

The responses of both the ARMON and G2301 analyzers are influenced by the air sample humidity level. Water correction factors for both instruments are empirically determined and corrected following Grossi et al. (2012) and Rella (2010), respectively.

190

2.2.2 Sample air drying system

195 The instruments used at the GIC3 station require a total flow of 2.5 L min^{-1} of sample air dried to a water concentration lower than 1000 ppm to perform simultaneous measurements of GHGs and ^{222}Rn concentrations. In the GIC3 inlet system, as shown in Figure S3 of the supplement, the sample air is passed through a Nafion® membrane (Permapure, PD-100T-24MPS) that exchanges water molecules with a dry counter-current air flow. The counter-current air flow is dried in a two-step process, first through a cooling coil in a refrigerator at $3 \text{ }^\circ\text{C}$ and a pressure of 5.5 barg, and then a cryotrap is used at -
200 $70 \text{ }^\circ\text{C}$ and a pressure of 1.5 barg. Multiple cryotrap are selected with electrovalves in order to increase the autonomy of the system to about 2 months. The typical water content of sample air inside the instruments is between 100 and 200 ppm.

2.2.3 Meteorological observations

205 Meteorological variables are continuously measured at the GIC3 tower. The canopy around the tower is below 20 m. The area surrounding the GIC3 station is hilly as shown on the topographic map of Figure S1 of the supplement. The tower is equipped with: (1) Two-dimensional sonic anemometer (WindSonic, Gill Instruments) for wind speed and direction (accuracies of $\pm 2 \%$ and $\pm 3 \text{ }^\circ$, respectively); (2) Humidity and temperature probe (HMP 110, Vaisala) with an accuracy of $\pm 1.7 \%$ and $\pm 0.2 \text{ }^\circ\text{C}$, respectively; (3)
210 Barometric pressure sensor (61302V, Young Company) with an accuracy of 0.2 hPa (at $25 \text{ }^\circ\text{C}$) and 0.3 hPa (from -40 to $+60 \text{ }^\circ\text{C}$). All the accuracies refer to the manufacturer's specifications.

2.3 Planetary boundary layer height (PBLH)

215 Planetary boundary layer height (PBLH) data used in this analysis have been extracted from the operational high resolution atmospheric model of the European Centre for Medium-Range Weather Forecasting (ECMWF-HRES) (ECMWF, 2006) for the period of interest (January 2013 - December 2015) for the GIC3 area. This model stores output variables every 12 hours (at 00.00 UTC and 12.00
220 UTC) with a temporal resolution output of 1 h and with forecasts from +00h to +11h. The horizontal spatial resolution of the model is about 16 km. In the ECMWF-HRES model the calculation of the PBLH is based on the bulk Richardson number (Ri) (Troen and Mahrt, 1986). As regards the reliability of modelled PBLH data, Seidel et al., (2012) have shown that data limitations in vertical profiles introduce height uncertainties that can exceed 50% for shallow boundary layers ($<1 \text{ km}$), but are generally $<20\%$
225 for deeper boundary layers. In addition, they compared radiosonde observations with re-analysis and climate models and showed that these latter two produce deeper layers due to the difficulty in simulating stable conditions.

2.4 CH₄ fluxes

2.4.1 CH₄ fluxes based on FLEXPART footprints and the Radon Tracer Method

235 The RTM is a well-known method (e.g. Hammer and Levin 2009) and it has been used in this study,
following Vogel et al. (2012) in order to obtain observation-based estimates of nocturnal CH₄ fluxes at
GIC3. The RTM uses atmospheric measurements of ²²²Rn and measured, or modelled, values of ²²²Rn
fluxes together with atmospheric mixing ratios of a gas of interest, i.e. CH₄, in order to retrieve the net
240 fluxes of this gas (e.g. Hammer and Levin 2009; Grossi et al., 2014). This method is based on the
assumption that the nocturnal lower atmospheric boundary layer can be described as a well-mixed box of
air (Schmidt et al. 1996; Levin et al., 2011; Vogel et al., 2012). The boundary layer is considered
homogeneous within the box and with a time varying height. No significant horizontal advection is
considered due to stable atmospheric conditions (Griffiths et al., 2012). In this atmospheric volume the
245 variation of the concentration of any tracer (shown with the subindex *i*) with time $C_i(t)$ will be
proportional to the flux of the tracer $F_i(t)$ and inversely proportional to the height of the boundary layer
 $h(t)$ (Eq.1; e.g. Galmarini, 2006; Griffiths et al., 2012; Vogel et al., 2012; Grossi et al., 2014).

$$\frac{dC_i(t)}{dt} \propto F_i(t) \cdot \frac{1}{h(t)} \quad (1)$$

250 Applying Eq. 1 for both ²²²Rn and CH₄. Eq. 2 is obtained, with a dimensionless conversion factor *c*
derived from the observed slope of the concurrent concentration increase of both gases:

$$\frac{\frac{dC_{CH_4}(t)}{dt}}{\frac{dC_{^{222}Rn}(t)}{dt}} \cdot F_{^{222}Rn} = c \cdot F_{^{222}Rn} = FR_{CH_4} \quad (2).$$

255 Observing the concentration increase of two gases that fulfil the above assumptions, here CH₄ and ²²²Rn.
If the flux of ²²²Rn is known, then the flux of CH₄ can be calculated (Levin et al., 2011). A description of
the specific criteria used to implement the RTM can be found in detail in Vogel et al. (2012). Grossi et al.
(2014) previously applied the RTM for the first time at the GIC3 station using only a 3-month dataset and
with a constant (in time and space) ²²²Rn flux of 60 Bq m⁻² h⁻¹. Here, in order to apply the RTM to
260 retrieve a time series of CH₄ fluxes (FR_{CH₄}) during 2013-2015 at the GIC3 station and to compare these
results with those obtained using a bottom-up inventory for methane (FE_{CH₄}), we used the following
extensive set-up:

1. A nocturnal window between 20.00 UTC and 05.00 UTC was selected for each single night
265 analysis in order to utilize only accumulation events when atmospheric concentrations of both
CH₄ and ²²²Rn had a positive concentration gradient due to positive net fluxes under stable
boundary layer conditions;

2. A data selection criterion based on a threshold of $R^2 \geq 0.8$ for the linear correlation between ^{222}Rn and CH_4 was used to reject events with low linear correlation between the atmospheric concentrations of both gases;
3. An *effective* radon flux influencing the GIC3 station each night from 2013 to 2015 was calculated by coupling local radon flux data, obtained using the output for the local pixel containing the GIC3 station of the model developed by López-Coto et al. (2013), with the footprints calculated by ECMWF-FLEXPART model (version 9.02) (Stohl, 1998). Local radon flux data were calculated as explained in the following paragraph, while the footprints obtained are described in Section 2.4.3.

The radon flux model of Huelva University (from now on named the UHU model) employed in this work has been described in detail by López-Coto et al. (2013). By using this model, a time-dependent inventory was calculated for the period 2011–2014 by employing several dynamic inputs, namely soil moisture, soil temperature and snow cover thickness. These data were obtained directly from Weather Research and Forecasting (WRF) simulations (Skamarock et al., 2008). A domain of 97 x 97 grid cells centred on Spain with a spatial resolution of 27 x 27 km² and a temporal resolution of 1 hour was defined. ^{222}Rn flux data calculated using this model were only available until November 2014 due to a lack of WRF simulations. In order to obtain data for this period when modelled ^{222}Rn flux data were not available, from December 2014 to December 2015, a seasonal and monthly climatology was calculated by using the UHU data set model for the years 2011-2014. Karstens et al. (2015) compared the ^{222}Rn flux values calculated over Europe by their model to UHU values and to long-term direct measurements of ^{222}Rn exhalation rates in different areas of Europe. They found a generally 40% higher ^{222}Rn exhalation rate on their map than estimated by the UHU map over Europe. This previous result has been taken into consideration within the present study to better interpret the obtained data.

2.4.2 CH₄ fluxes based on FLEXPART footprints and the EDGARv4.2 inventory grid map

Bottom-up CH_4 fluxes influencing the GIC3 station were estimated by using the footprints calculated by the ECMWF-FLEXPART model (obtained as described in Section 2.4.3) and the Emissions Database for Global Atmospheric Research (EDGAR) version 4.2 (EDGAR, 2010). The EDGAR inventory, developed by the European Commission Joint Research Centre and the Netherlands Environmental Assessment Agency, includes global anthropogenic emissions of GHGs and air pollutants by country on a spatial grid. The EDGAR version used in the present study provides global annual CH_4 emissions on a 0.1 degree (11 km) resolution for the year 2010. All major anthropogenic source sectors, e.g. waste treatment, industrial and agricultural sources (e.g. enteric fermentation) are included, whereas natural sources (e.g. wetlands or rivers) are not. The spatial allocation of emissions on 0.1 degree by 0.1 degree grid cells in EDGAR has been built up by using spatial proxy datasets with the location of energy and manufacturing facilities, road networks, shipping routes, human and animal population density and agricultural land use. UNFCCC reported national sector totals are then removed with the given percentages of the spatial proxies over the country's area (EDGAR, 2010). Figure 1 shows the EDGAR inventory grid map extracted for Spain.

The influence of the emissions associated with the cities surrounding the region of GIC3 was also modelled using this inventory to better understand their impact. In Table S1 of the supplement the coordinates of the upper and lower corners of the areas used to describe the location of the metropolitan areas over the EDGAR inventory are reported.

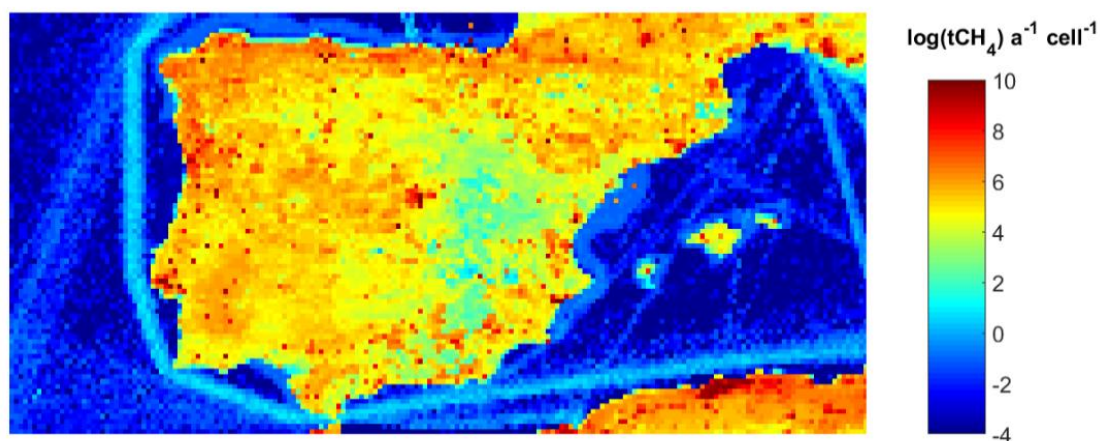


Figure 1. CH₄ EDGARv4.2 inventory grid map extracted for Spain (year 2010).

2.4.3 Footprints

The Lagrangian particle dispersion model FLEXPARTv9.0.2 has been extensively validated and is nowadays widely used by the scientific community to calculate atmospheric source-receptor relationships for atmospheric gases and organic particles (e.g. Stohl, 1998; Stohl et al., 2005; Arnold et al., 2010; Font et al., 2013; Tohjima et al., 2014). FLEXPART allows computation of the trajectories of virtual air parcels arriving at the receptor point, i.e. the GIC3 station, at a specific time. FLEXPART has been applied here to calculate 24 h backward trajectories of 10,000 virtual air parcels starting at 00.00 UTC for each night of the period 2013-2015. Each back trajectory simulation was run with a time-step output of 3 h. Meteorological data from the operational ECMWF-HRES model with a resolution of 0.2 degrees were used as input fields for the FLEXPART modelling. The FLEXPART output domain resolution was 0.2 degrees. The domain was set at (25°N, 40°W) for the lowest left corner and (65°N, 10°W) for the upper right corner. A nested output domain of 0.05 degrees resolution was defined at (37°N, 12°W) for the lowest left corner and (43°N, 0°E) for the upper right corner. The FLEXPART model accounts for both the vertical and horizontal position of the virtual air parcels and their residence time in each grid cell. This information allows the influence of atmosphere-surface exchange to be estimated on the observed concentrations if air parcels are within the boundary layer. A maximum height of 300 m a.g.l. has been selected for the footprint analysis following Font et al. (2013). The average nocturnal footprint for the period 2013-2015 is presented in Figure 2. The footprints obtained for the nested FLEXPART domain were combined with the EDGAR inventory map for CH₄ emissions (EDGAR, 2010) and with the UHU ²²²Rn flux inventory map (López-Coto et al., 2013), separately, in order to obtain the time series of

modelled CH₄ and *effective* ²²²Rn fluxes. The resulting mean flux $F_i(S, t_n)$, for each gas i , at the receptor S (GIC3 station) and for each night t_n , with n ranging over the 3-year period, is thus given by Eq. 3:

$$F_i(S, t_n) = \sum_{t=t_{n,n}}^{t=t_n} \sum_x F_i(x, t_n) * w(x, T) \quad (3)$$

where t ranges between the 24h of back-trajectories, $F_i(x, t)$ denotes the flux of a given grid cell x at time t derived from the EDGAR or UHU inventory map, separately. The weighting factor of each grid cell $w(x, T)$ is calculated using the FLEXPART footprint for each night t_n over the 3-year period and it has
 345 been calculated by normalizing the residence time of each grid cell over the nested domain and during the 24 h back-trajectories (T), as given by Eq. 4:

$$\sum_{x,t}^T w(x, t) = 1 \quad (4)$$

350

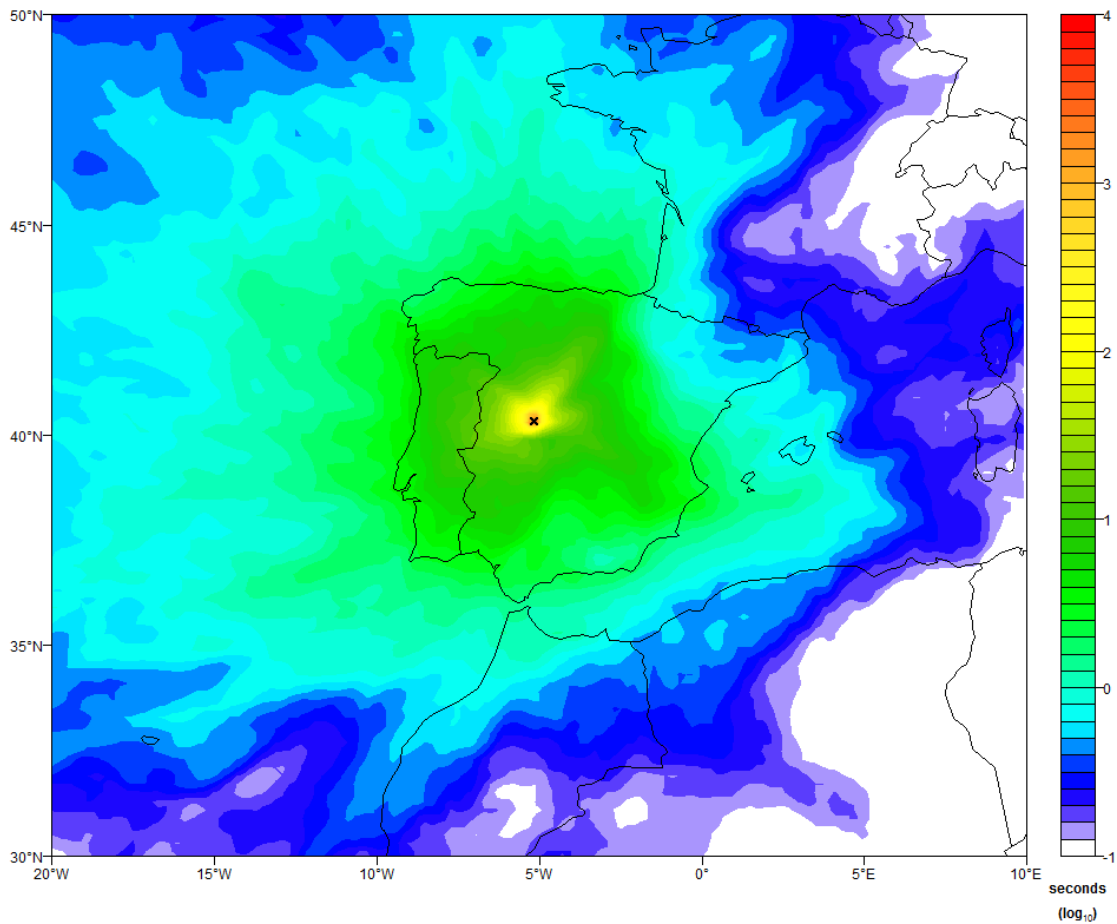


Figure 2. Average nocturnal FLEXPART footprint for the 2013-2015 period (residence time t is on the logarithmic scale).

355

3 Results

In this section we present the results of the daily and seasonal atmospheric CH₄ variability at GIC3 station analysed using a record of 3-year hourly CH₄ and ²²²Rn time series. Unfortunately, due to problems in the air sample system, data for 11 % of the time period are not available, mainly in the summer of 2013.

Grossi et al. (2016) presented a complete characterization of the main meteorological conditions and ²²²Rn behaviour at the ClimaDat stations including GIC3, and we will use these previous results to interpret atmospheric processes and the variability of CH₄ mixing ratio, as well as to understand the dominating wind regimes for CH₄ flux data analysis (Figure S4 of the supplement presents the monthly wind regimes observed at the GIC3 station both for daytime and night-time).

3.1. Statistics of the daily and seasonal atmospheric CH₄ variability

The 3-year hourly time series of atmospheric CH₄ mixing ratios measured at GIC3 shows a median value of 1904.5 nmol mol⁻¹ with an absolute deviation of 29.6 nmol mol⁻¹. The boxplots in Figure 3 present the medians of the atmospheric CH₄ mixing ratios and ²²²Rn concentrations measured at the GIC3 station over the dataset on an hourly (left panels) and a monthly (right panels) basis. Monthly means have been calculated separately for daytime (07.00 UTC – 18.00 UTC) and night-time (19.00 UTC – 06.00 UTC).

375

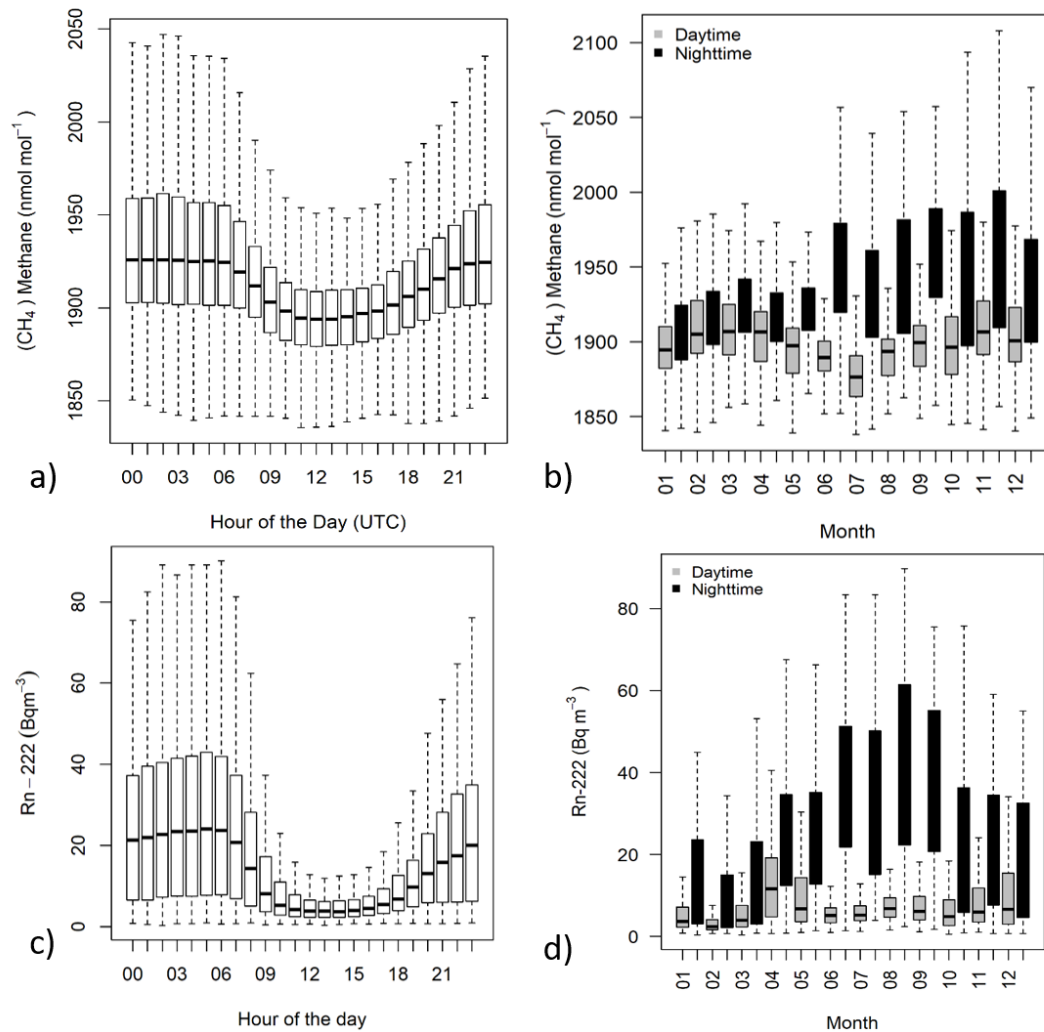


Figure 3. Boxplots of hourly (a,c) and monthly (b,d) atmospheric CH₄ mixing ratios (a,b) and ²²²Rn concentrations (c,d) measured from January 2013 to December 2015 at the GIC3 station. For each median (black bold line) the 25th (Q1; lower box limit) and 75th (Q3; upper box limit) percentiles are reported in the plot. The lower whisker goes from Q1 to the smallest non-outlier in the data set, and the upper whisker goes from Q3 to the largest non-outlier. Outliers are defined as >1.5 IQR or <1.5 IQR (IQR: Interquartile Range).

385

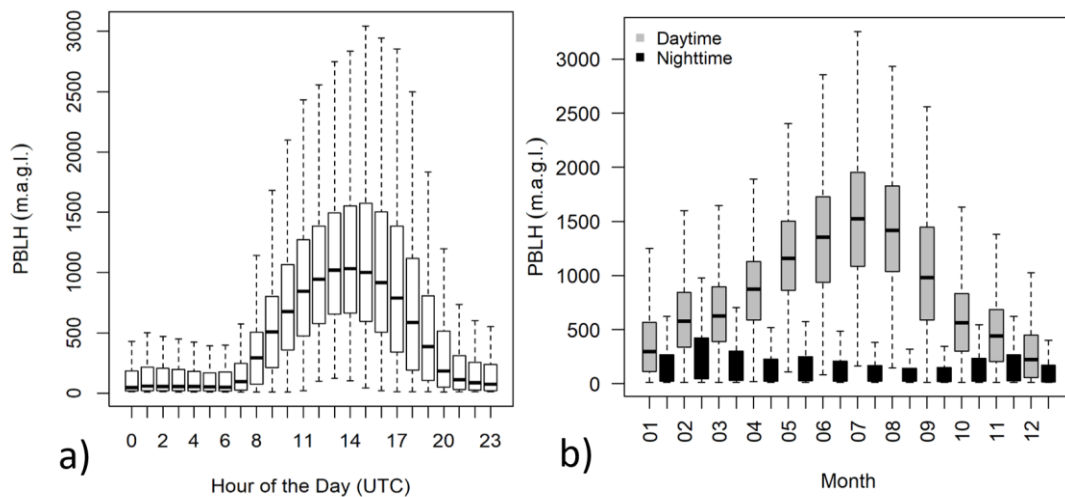
The maximum hourly median methane mixing ratio measured within the 3-year observation period is 1921.1 nmol mol⁻¹ and is observed at 03.00 UTC, whereas the minimum hourly median value of 1889.9 nmol mol⁻¹ is observed at 13.00 UTC. The absolute standard deviation of the hourly median is 16.97 nmol mol⁻¹. The hourly median daily amplitude at this station, between the minimum and the maximum, is 31.18 nmol mol⁻¹. CH₄ concentrations usually start decreasing at GIC3 in the morning at around 07.00 UTC and 08.00 UTC and begin to increase again in the afternoon at around 17.00 UTC and 18.00 UTC. Night-time CH₄ concentrations present an absolute standard deviation of 60 nmol mol⁻¹, while for daytime concentrations it is 30 nmol mol⁻¹. The same pattern is observed in the daily cycle of atmospheric ²²²Rn (Grossi et al., 2016). Monthly daytime and night-time medians of CH₄ mixing ratios and ²²²Rn concentrations show different patterns, as seen in Figure 3 (B,d). The night-time monthly medians of

395

methane mixing ratio measured in the months between June and December look higher than those measured between January and May. Night-time monthly medians of measured ^{222}Rn concentration are highest between July and August.

400 3.2 Daily and seasonal PBLH variability

Figure 4 shows the hourly median (a) and the monthly median (b) variability of the PBLH data extracted from the ECMWF-HRES model for the grid containing the GIC3 station. On a daily basis the hourly median of the PBLH reaches its minimum during night-time between 23.00 UTC and 07.00 UTC. The PBLH starts to increase at around 08.00 UTC, reaching its maximum between 14.00 UTC and 16.00 UTC and then decreases again after 17.00 UTC. On a monthly basis, the daytime monthly median PBLH reaches its minimum during the winter months of January and December, while it reaches its maximum in the summer months. The highest night-time monthly medians for the PBL heights are observed in winter. The daytime monthly PBLH medians present a quite symmetric distribution (around July as a centre-line), similar to the night-time monthly ^{222}Rn medians (Figure 3d).



415 Figure 4 Boxplots of hourly (a) and monthly (b) PBLH data extracted from the ECMWF-HRES model for the period January 2013 - December 2015 at the GIC3 station. For each median (black bold line) the 25th (Q1; lower box limit) and 75th (Q3; upper box limit) percentiles are reported in the plot. The lower whisker goes from Q1 to the smallest non-outlier in the data set, and the upper whisker goes from Q3 to the largest non-outlier. Outliers are defined as >1.5 IQR or <1.5 IQR (IQR: Interquartile Range).

420

425 **3.3 Comparison between CH₄ and ²²²Rn variability**

A comparison of the daily and seasonal variability of the atmospheric concentrations of ²²²Rn and CH₄ in relation to changes in height of the PBL at the GIC3 station (2013-2015) is presented in Figures 5 and 6, respectively.

430

The daily evolution of hourly means of the ²²²Rn atmospheric concentrations (Figure 5, upper panel) implies that on a daily time-scale, when ²²²Rn flux can be considered fairly constant (e.g. López-Coto et al., 2013), PBLH variations drive the increase or decrease of the atmospheric ²²²Rn concentrations. In this sense, ²²²Rn seems to be an excellent predictor of PBLH (and vice-versa) on a daily time-scale. Looking

435 at the hourly means of the atmospheric CH₄ mixing ratios (Figure 5, lower panel), we can observe that methane decreases as the PBLH increases, as was observed for ²²²Rn. However, between 12.00 UTC and 18.00 UTC higher values in CH₄ mixing ratios relative to the values observed between 10.00 UTC and 12.00 UTC are observed, which have similar PBLH conditions and could indicate some daily variability in the methane fluxes.

440

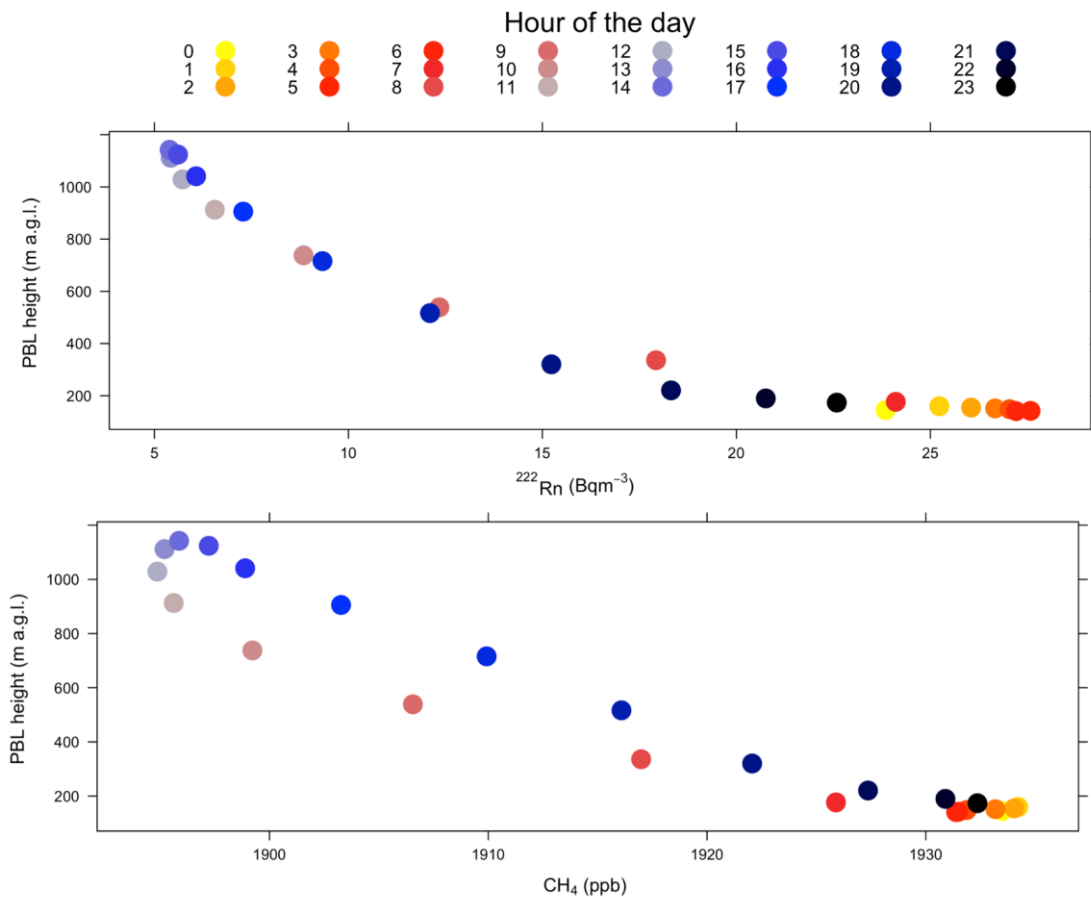


Figure 5 Relation between hourly means of atmospheric CH₄ (lower panel) and ²²²Rn (upper panel) concentrations measured during 2013-2015 at the GIC3 station and ECMWF data of PBLH for the same area and for the same time interval.

445

To interpret the monthly variability, the daily amplitude for each gas, i.e. $\Delta^{222}\text{Rn}$ for radon and ΔCH_4 for methane, was calculated in order to subtract the influence of the changing daily background contribution measured at the GIC3 station. $\Delta^{222}\text{Rn}$ is defined as the difference between average night-time concentration data (19.00 UTC - 06.00 UTC) versus average daytime (07.00 UTC-18.00 UTC) concentration data (Eq. 5). ΔCH_4 has been calculated accordingly.

$$\Delta^{222}\text{Rn} = {}^{222}\text{Rn}_{\text{nighttime}} - {}^{222}\text{Rn}_{\text{daytime}} \quad (5)$$

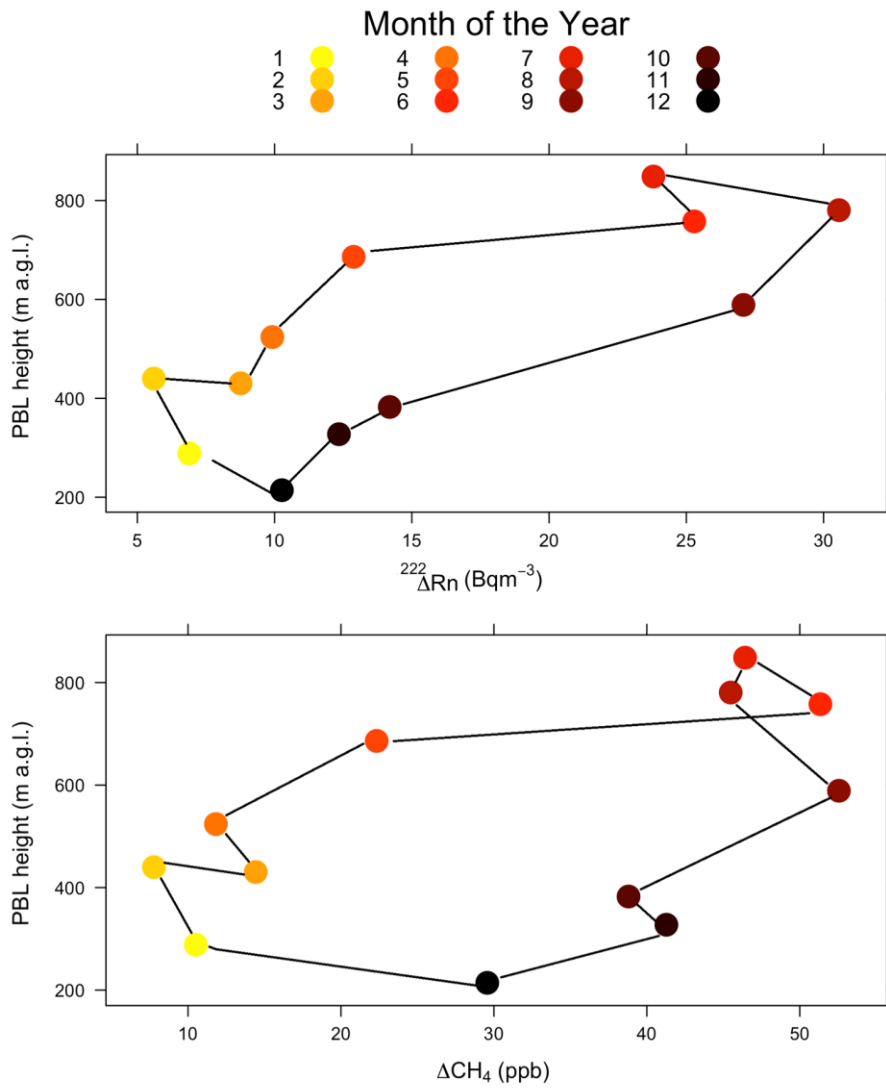
Figure 6 reveals that monthly amplitudes increase in summer, when the daytime PBLH increases very strongly due to vertical mixing (see Figure 4). This general tendency is found both for ^{222}Rn and CH_4 concentrations. ^{222}Rn concentrations amplitudes in autumn are higher than in winter under the same PBLH conditions (Figure 6, upper panel). This could indicate that some process, other than PBLH, is driving this difference in the ^{222}Rn concentrations. In Figure 7 we observe how the monthly ^{222}Rn flux calculated by the UHU model (presented in Section 2.4) changes.

460

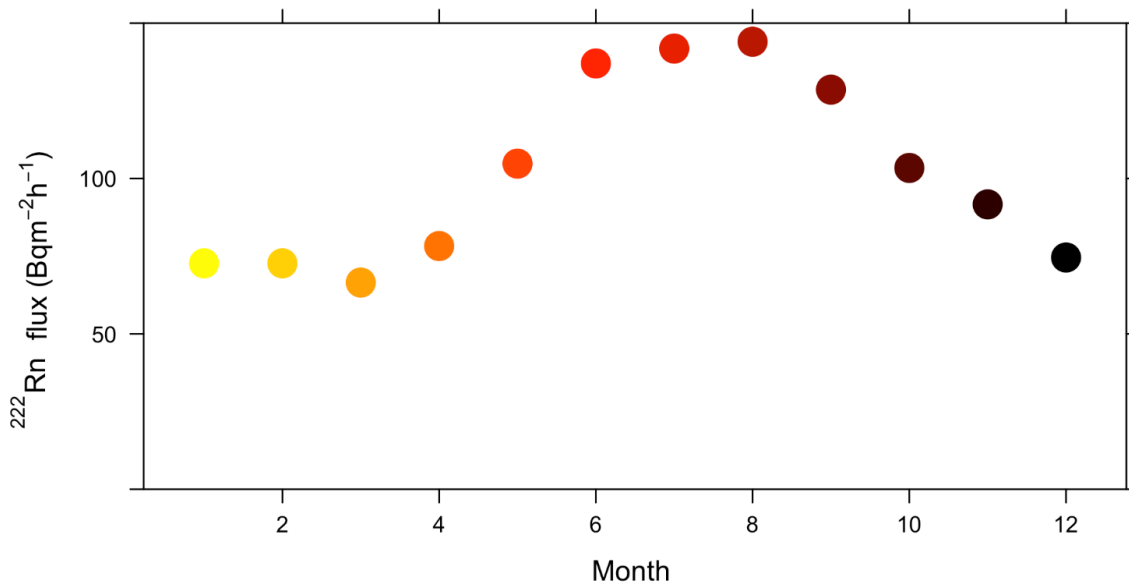
In agreement with Grossi et al. (2016), we find a lower ^{222}Rn flux at GIC3 during winter due to snow cover events and low temperatures, which prevent ^{222}Rn diffusion from the soil. The ^{222}Rn flux then increases almost two-fold and three-fold during the autumn and summer months, respectively. This is due to drier soil conditions and the high gradient of temperature in the surface atmospheric layer which facilitates the escape of ^{222}Rn from the pores of the granitic soil (Nazaroff and Nero, 1988). This seasonality of the ^{222}Rn flux could be the main cause of the increased atmospheric $\Delta^{222}\text{Rn}$ under the same PBLH conditions.

Monthly variations of ΔCH_4 shown in Figure 6 (bottom panel) display no clear simple correlation with PBLH. ΔCH_4 appears to be higher between the months of June and December irrespective of the corresponding PBLH values.

470



475 Figure 6. Relation between monthly means of concentration amplitudes of ΔCH_4 (bottom panel) and $\Delta^{222}\text{Rn}$ (upper panel) measured during 2013-2015 at the GIC3 station and monthly ECMWF data of PBLH for the same area during same time interval.



480 Figure 7. Monthly ²²²Rn flux means calculated by the UHU model and climatology for 2013-2015 at the GIC3 station. Coloured circles indicate the same months as in Figure 6.

3.4 Variations of CH₄ fluxes

485 So far, daily variations for both CH₄ mixing ratio and ²²²Rn concentrations can be mainly explained in relation to the accumulation or dilution of gas concentration within the PBL. However, the hysteresis observed for the CH₄ mixing ratio of Figure 5 (bottom panel) seems to indicate a small change in the methane source between 12.00 UTC and 18.00 UTC.

490 Monthly $\Delta^{222}\text{Rn}$ variability can be understood when we account for seasonal ²²²Rn flux changes. Unfortunately, existing emission inventories (EDGAR, 2010; MMA, 2016) generally do not yet provide seasonally, hourly varying CH₄ emission values either for Europe in general or for Spain in particular.

In order to understand the impact that temporal changes of CH₄ emissions may have on monthly mean
 495 atmospheric CH₄ mixing ratios, we have applied two different methodologies, as explained in Sections 2.4.1 and 2.4.2 and we have compared their resulting fluxes: FR_CH₄ and FE_CH₄, respectively. Figure 8 presents the *effective* ²²²Rn flux time series used for the application of the first methodology (RTM), together with the raw ²²²Rn flux calculated by the UHU model and its seasonal climatology.

500

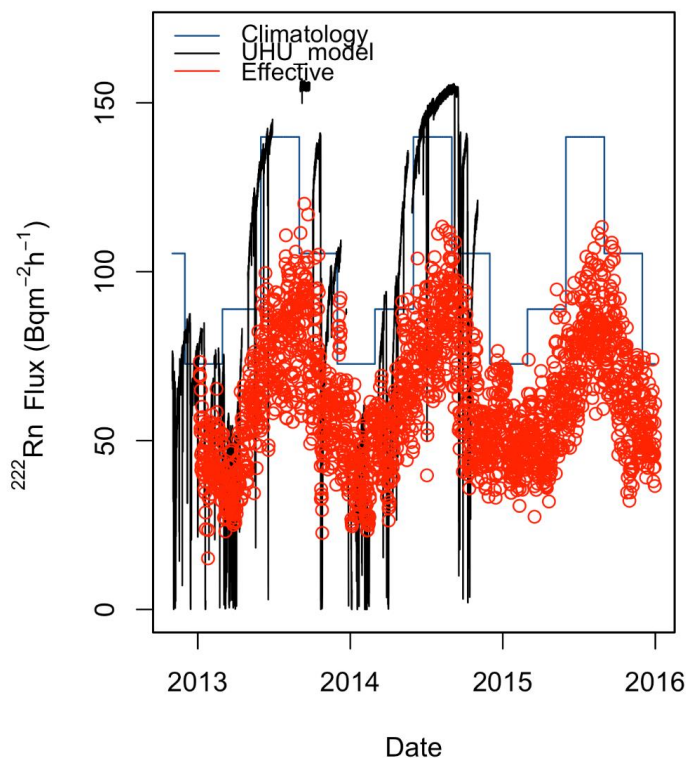


Figure 8. Time series of local ^{222}Rn flux calculated by the UHU model (black line; López-Coto et al. (2013)) for the GIC3 area, ^{222}Rn flux seasonal climatology (blue line) and *effective* ^{222}Rn flux calculated on the basis of FLEXPART footprints (red dots). This last series was used within the RTM method.

505

Figure 9 presents the time series of CH_4 fluxes estimated at the GIC3 station and T_i (grey shaded rectangles) indicates the time when transhumant livestock returns to the GNP after spending the winter in the south of Spain (Tapias, 2014; Rodríguez, 2015). The green shaded areas indicate the periods, between June and December, when transhumant livestock typically stays in the GIC3 region (Ruiz Perez and Valero Sáez, 1990; López Sáez et al., 2009; Libro Blanco, 2013). Data coverage in the second part of the time-series (2014-2015) is higher than in the first period (2013-2014) because the simultaneous availability of ^{222}Rn and CH_4 data was higher. The mean of FR_CH_4 fluxes over the dataset is $0.11 \text{ mg CH}_4 \text{ m}^{-2} \text{ h}^{-1}$ with 25th and 75th percentiles of $0.07 \text{ mg CH}_4 \text{ m}^{-2} \text{ h}^{-1}$ and $0.14 \text{ mg CH}_4 \text{ m}^{-2} \text{ h}^{-1}$, respectively. The mean of FE_CH_4 fluxes over the dataset is $0.33 \text{ mg CH}_4 \text{ m}^{-2} \text{ h}^{-1}$ with 25th and 75th percentiles of $0.28 \text{ mg CH}_4 \text{ m}^{-2} \text{ h}^{-1}$ and $0.36 \text{ mg CH}_4 \text{ m}^{-2} \text{ h}^{-1}$, respectively. FR_CH_4 fluxes are constantly lower than FE_CH_4 fluxes, although this discrepancy decreases during some periods, as we will investigate later. FEC_CH_4 fluxes obtained with the EDGARv4.2 inventory by considering only the contribution of the cities that are located around the GIC3 station, in agreement with the masks presented in Table S1 of the supplement material, had a total mean value over the dataset of $0.02 \text{ mg CH}_4 \text{ m}^{-2} \text{ h}^{-1}$ with 25th and 75th percentiles of $0 \text{ mg CH}_4 \text{ m}^{-2} \text{ h}^{-1}$ and $0.006 \text{ mg CH}_4 \text{ m}^{-2} \text{ h}^{-1}$, respectively.

520

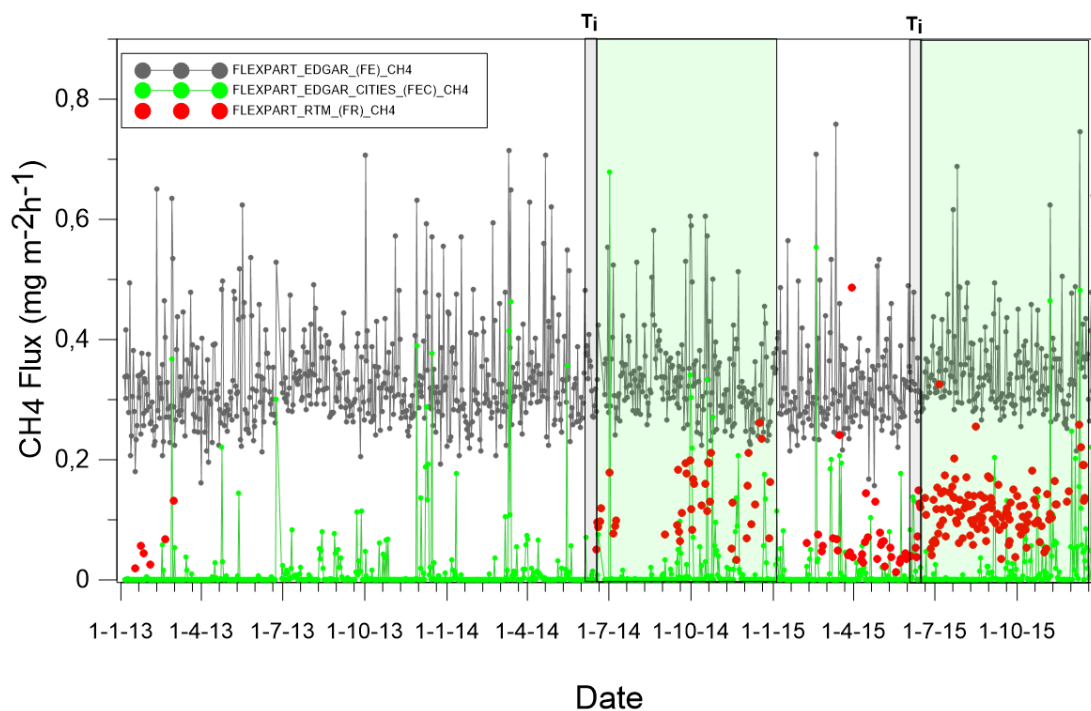
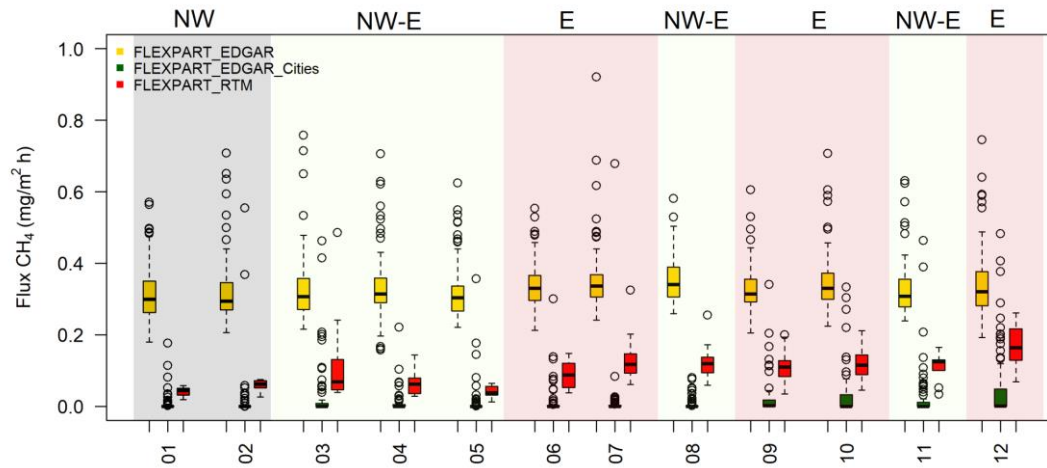


Figure 9 Results of night-time FR_{CH₄} fluxes (mg CH₄ m⁻² h⁻¹) (red circles) obtained at the GIC3 station
 525 from January 2013 to December 2015 compared with night-time FE_{CH₄} fluxes obtained using bottom-
 up inventory emissions (grey line) and calculated FEC_{CH₄} fluxes from contributions from surrounding
 cities (green circles). The weeks T₁ represent the period of 2014 (21st-27th June) and 2015 (20th-26th June)
 when transhumant livestock returned to the GIC3 area after spending the winter in the south of Spain and
 concurrent with the availability of FR_{CH₄} fluxes data. Shaded green regions represent the periods when
 530 transhumant livestock remain in the GIC3 area.

Figure 10 shows monthly boxplots of FE_{CH₄} and FR_{CH₄} fluxes. Shaded areas are coloured according
 to the main local wind directions reaching the GIC3 station at night. This classification is based on the
 results presented in Figure S2 of the supplementary material, where monthly windrose plots for the GIC3
 535 station between 2013-2015 are shown. We can observe that there is no variability in monthly FE_{CH₄}
 flux values. In contrast, FR_{CH₄} flux results show an increase of CH₄ fluxes between June and December
 that seems to be independent of the seasonally changing dominant wind directions. This increase is also
 uncorrelated with seasonally changing ²²²Rn fluxes (Figure 7). The seasonal change of CH₄ fluxes
 between the first and the second half of the year at GIC3 could indeed be related to variations in local
 540 CH₄ emissions. The period between June and December represents the time of year when transhumant
 livestock returns to the GNP.

The contribution of cities is only visible during certain months and it seems to be related with winds
 coming from the east in the direction of the Madrid urban area (see Figure S2 of the supplement material).



545

Figure 10 Boxplots of monthly CH_4 fluxes ($\text{mg CH}_4 \text{ m}^{-2} \text{ h}^{-1}$) calculated for the GIC3 area using the RTM technique (red) and the EDGAR inventory (total in yellow; contribution of cities in green). Coloured areas indicate main wind directions for specific months. For each median (black bold line) the 25th (Q1; lower box limit) and 75th (Q3; upper box limit) percentiles are reported in the plot. The lower whisker goes from Q1 to the smallest non-outlier in the data set, and the upper whisker goes from Q3 to the largest non-outlier. Outliers are defined as $>1.5 \text{ IQR}$ or $<1.5 \text{ IQR}$ (IQR: Interquartile Range).

550

The disagreement observed between FE_CH_4 and FR_CH_4 fluxes in the months between June and December (Figures 9 and 10), when the transhumant livestock is in the GIC3 area, may be due to different reasons: i) a possible underestimation of the ^{222}Rn flux outputs from the UHU radon flux model, which would lead to lower FR_CH_4 fluxes (Equation 2). As explained previously, Karstens et al., 2015 compared their radon flux model with the UHU model and it gave, generally, 40 % higher ^{222}Rn flux values than the UHU model over Europe; ii) the methodology used within the EDGAR for the spatial disaggregation of national sector emission over the country could lead to a distribution of CH_4 emission in the GIC3 region higher than true levels leading to an overestimation of the FE_CH_4 ; iii) the fixed height of 300 m used for the calculation of nocturnal footprints could introduce a bias. However, this value is well within the range of nocturnal PBLH values calculated with data extracted from the ECMWF-HRES model. Furthermore, the calculated FLEXPART footprints were used both for FR_CH_4 and FE_CH_4 calculations and this should not affect the relative differences between their values.

560

565

When applying a 40% increase for the local ^{222}Rn source, as suggested by Karstens et al., 2015, we can re-calculate FR_CH_4 emissions as $\text{FR_CH}_4_{\text{rescale}}$. The boxplot of the monthly medians of FE_CH_4 , FR_CH_4 and $\text{FR_CH}_4_{\text{rescale}}$ are compared in Figure 11. The mean of $\text{FR_CH}_4_{\text{rescale}}$ fluxes over the dataset is $0.29 \text{ mg CH}_4 \text{ m}^{-2} \text{ h}^{-1}$ with 25th and 75th percentiles of $0.17 \text{ mg CH}_4 \text{ m}^{-2} \text{ h}^{-1}$ and $0.34 \text{ mg CH}_4 \text{ m}^{-2} \text{ h}^{-1}$, respectively. $\text{FR_CH}_4_{\text{rescale}}$ is in agreement with FE_CH_4 fluxes during the months between June and December, when the transhumant livestock remains in the GIC3 area (Cattle season).

570

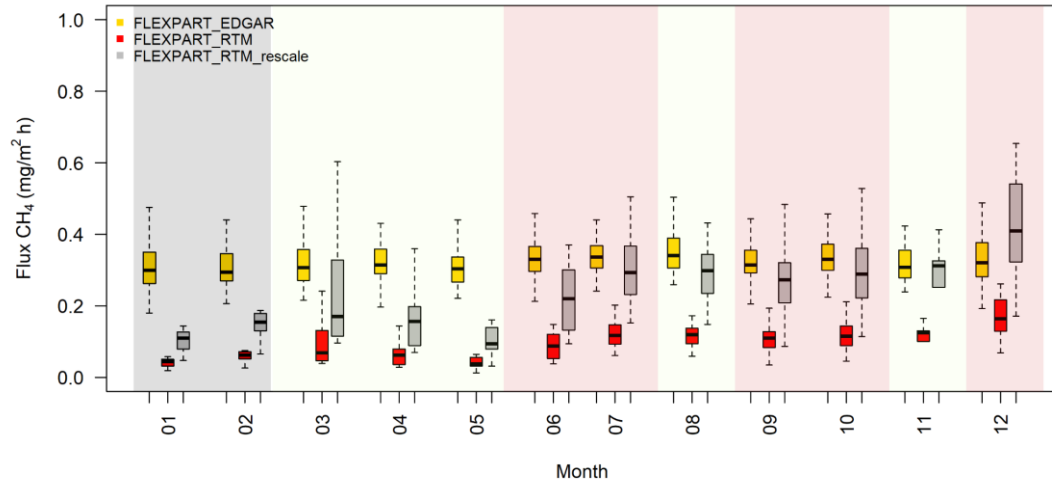
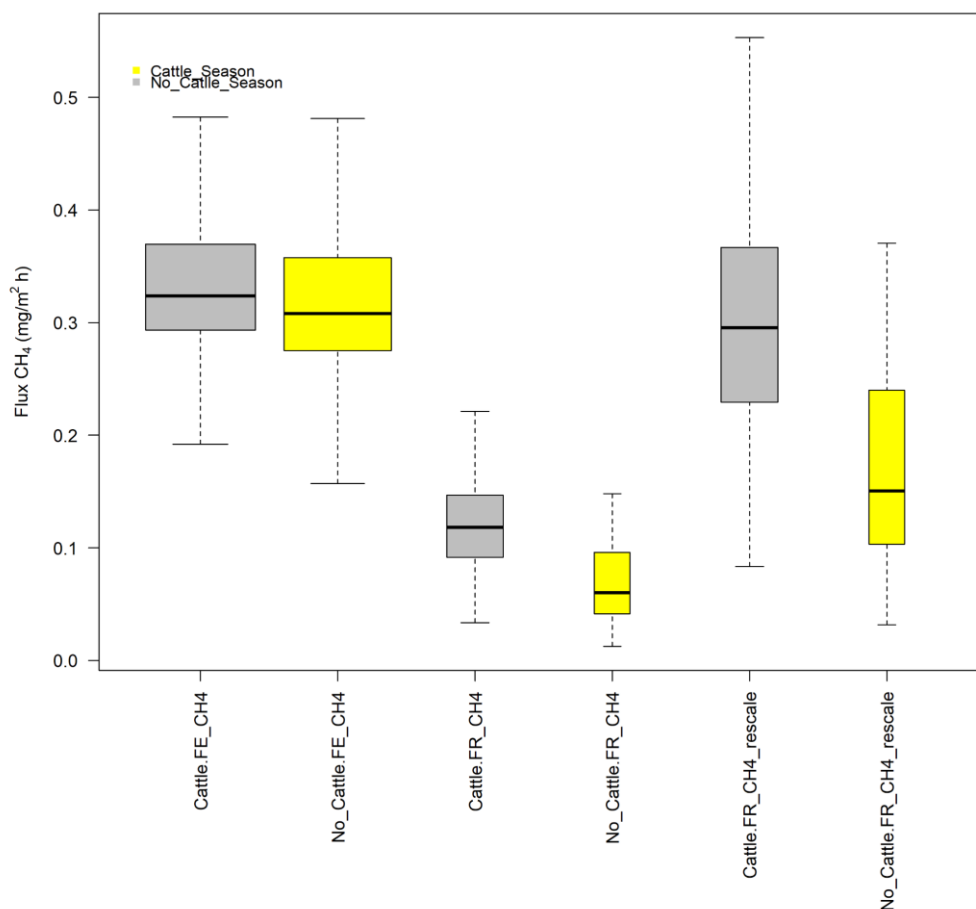


Figure 11, Boxplots of monthly CH₄ fluxes (mg CH₄ m⁻² h⁻¹) calculated for the GIC3 area using the RTM technique (red), the EDGAR inventory (yellow) and RTM technique using the ²²²Rn flux comparison factor found by Karstens et al., 2015 (grey). Coloured areas indicate main wind directions for specific months. For each median (black bold line) the 25th (Q1; lower box limit) and 75th (Q3; upper box limit) percentiles are reported in the plot. The lower whisker goes from Q1 to the smallest non-outlier in the data set, and the upper whisker goes from Q3 to the largest non-outlier. Outliers are defined as >1.5 IQR or <1.5 IQR (IQR: Interquartile Range).

To highlight seasonal differences, FE_CH₄, FR_CH₄ and FR_CH₄_rescale fluxes are aggregated into two boxplots in Figure 12, according to the No-Cattle season (January until May), when there is no livestock in the GIC3 area, and Cattle season (June until December). According to these data during the No-Cattle season, FR_CH₄ fluxes present a mean value of 0.09 CH₄ m⁻² h⁻¹ with a standard deviation of 0.15 mg CH₄ m⁻² h⁻¹. During the Cattle season, the mean value of FR_CH₄ fluxes is 0.12 CH₄ m⁻² h⁻¹ with a standard deviation of 0.05 mg CH₄ m⁻² h⁻¹. The mean value of FR_CH₄_rescale fluxes is 0.24 mg CH₄ m⁻² h⁻¹ during the No-Cattle season with a standard deviation of 0.39 mg CH₄ m⁻² h⁻¹ and it is 0.30 mg CH₄ m⁻² h⁻¹ during the Cattle season with a standard deviation of 0.12 mg CH₄ m⁻² h⁻¹. The corresponding values for FE_CH₄ fluxes are 0.31 mg CH₄ m⁻² h⁻¹ for the No-Cattle season and 0.32 mg CH₄ m⁻² h⁻¹ for the Cattle season.



595 Figure 12. Boxplots of FE_CH₄, FR_CH₄ and FR_CH₄corr fluxes (in mg m⁻² h⁻¹) calculated for the GIC3
 area during the “warm” season (June-December, yellow box) and the “cold” season (January-May, grey
 box). For each median (black bold line) the 25th (Q1; lower box limit) and 75th (Q3; upper box limit)
 percentiles are reported in the plot. The lower whisker goes from Q1 to the smallest non-outlier in the
 data set, and the upper whisker goes from Q3 to the largest non-outlier. Outliers are defined as >1.5 IQR
 600 or <1.5 IQR (IQR: Interquartile Range).

4 Discussion

The present results show the different influences that meteorological conditions (PBLH and wind
 605 direction) and regional sources may have on the variability of atmospheric CH₄ concentrations observed
 at the GIC3 station. ²²²Rn observations have been used, together with modelled PBLH data, to better
 understand the reasons for the variability of the atmospheric CH₄ concentrations observed at the station
 for different times scales. The use of ²²²Rn as a tracer to calculate independent fluxes of GHGs has been
 shown in order to help with the improvement of emission inventories on a regional scale.

610

4.1 Daily variability of atmospheric CH₄ concentrations

The daily cycle of atmospheric CH₄ mixing ratios (Figure 3a) measured at GIC3 shows significant changes between daytime and night-time periods. The large increase of nocturnal CH₄ mixing ratios can
615 mainly be explained by the decreased height of the planetary boundary layer (Figure 4a), which is supported by a similar behaviour of ²²²Rn concentrations (Figure 3c). Indeed, CH₄, as well as ²²²Rn, reach their maximum concentration when the PBLH is below 300 m a.g.l. during the night, while their atmospheric concentrations decrease with the increase of the PBLH during daytime.

620 The correlation of PBLH and ²²²Rn (and CH₄) in Figure 5 indicates that ²²²Rn fluxes do not strongly vary on daily time-scales or, at least, not to a degree that can influence their atmospheric concentration variability. CH₄ fluxes seem to change on a daily time-scale. Average afternoon CH₄ concentrations are slightly enhanced compared to those from the morning for similar PBLH values (Figure 5, bottom panel). They show a hysteresis behaviour which could indicate local emissions increase or that a systematic
625 transport of CH₄ enhanced air-masses, not rich in radon, occurs at GIC3. Some studies (e.g. Bilek et al. 2001, Wang et al., 2015) have found strong emission increases of dairy cows post-feeding in feedlots, while McGinn et al. (2010) only found small diurnal increases of CH₄ emissions between 11h and 17h for grazing cattle. Unfortunately, no detailed information about the feeding cycle of the GIC3 livestock is available, but grazing should be considered the predominant form of livestock management in
630 transhumance. On the other hand, Figures 9 and 10 together with Figure S4 show the influences of eastern winds, coming from the Madrid direction, on the CH₄ fluxes.

4.2 Seasonal variability of atmospheric CH₄ concentrations

635 To understand the drivers of monthly changing concentrations of CH₄ we need to account for PBLH local meteorology, changing regional emissions and changing background concentrations of CH₄ at GIC3. Median monthly mixing ratios for daytime and night-time (Figure 3b) are discussed alongside Δ CH₄ (Figure 6) which allows us to subtract seasonal and synoptic background variations. This enables us to
640 focus on the impact of PBLH for individual days that are then averaged to investigate how Δ CH₄ changes on a monthly basis. The observed variability of Δ CH₄ (Figures 3b and 6) cannot be explained only in terms of changes of the PBLH. Monthly averages of Δ CH₄ (and night-time monthly CH₄ boxplots, Figure 3b) present their maximum values between June and December; and their minimum values during the rest of the months irrespective of the height of the PBL. From co-located ²²²Rn concentration observations we
645 learn that an increase in the average monthly fluxes (Figure 7) can compensate the effect of increased dilution in the deeper summer PBL on the observed concentrations (Figure 6, upper panel) yielding similar atmospheric ²²²Rn concentrations. The increase of the modelled ²²²Rn flux in the GIC3 region from the winter to autumn season and the following decrease can coherently help to explain the variation observed in monthly Δ ²²²Rn. Thus, the comparison between Δ CH₄ and Δ ²²²Rn suggests that there may
650 also be a monthly variability in the sources of CH₄ which should help to understand monthly atmospheric mixing ratios variability. This has been further confirmed by our FR_CH₄ flux estimates, as seen in Figures 9, 10 and 11. Of course, the FR_CH₄ flux estimates are limited to night-time due to the RTM

hypothesis. FR_CH₄ fluxes show a total mean value 33% lower than FE_CH₄ fluxes over the data set. When ²²²Rn fluxes are rescaled according to Karstens et al., 2015, this difference is drastically reduced to 10-15%.

RTM-based CH₄ fluxes show an increase of 25% during the second semester of the year on a monthly basis. This increase coincides with the period of the year when transhumant livestock resides in the GIC3 region. Although no exact information is available on the number of animals present only in the GIC3 area, during this period of enhanced ruminant emissions, the difference between CH₄ fluxes based on RTM and the EDGAR inventory is reduced from 73% to 65% for FR_CH₄ and from 27% to 9% for FR_CH₄_rescale. The difference during the No-Cattle season is likely due to the constant annual emission factor of CH₄ emission used within the bottom-up inventory which, of course, cannot yet reflect transhumance activity. The likely explanation is that all emissions from the aforementioned animals has been constantly allocated to this region, which is why FE_CH₄ is also larger than FR_CH₄_rescale during months when they are not present. The RTM analysis performed here suggests that transhumance could be a relevant process to understand sub-annual CH₄ emissions in the region and can affect the spatial distribution of CH₄ sources within a country. Our study, indicates that the choice of ²²²Rn model has an important impact on annual total emissions calculated, while seasonal and short-term patterns are preserved.

5 Conclusions and outlook

To gain a full picture of the Spanish (and European) GHGs balance, understanding of CH₄ emissions in different regions is a critical challenge as well as is the improvement of bottom-up inventories for all European regions. Our study uses, among others, GHGs, meteorological and ²²²Rn tracer data from one of the eight stations of the new ClimaDat network in Spain, which provides continuous atmospheric observations of CH₄ and ²²²Rn in a region of Europe. The present study underlines the fact that this data, combined with retrieved PBLHs data and atmospheric transport modelling (FLEXPARTv92) can help to understand the main causes of temporal variability of GHG mixing ratios and can offer new insights into regional emissions by identifying the impacts of changing sources, e.g. emissions from transient livestock.

These first promising results should lead to further application of this RTM to other GHG time series from the ClimaDat network and potentially in continent-wide networks such as ICOS that routinely perform co-located GHG and ²²²Rn observations. Particularly, the use of the RTM has been shown, while also highlighting the need to improve this method, especially in regard to: i) validation of the ²²²Rn flux maps applied within the RTM; ii) standardization of the footprint calculation.

Although the transhumant livestock seems to be the likely reason for the seasonal changes observed in the FR_CH₄ fluxes at the GIC3 station, other sources could also contribute to this seasonality such as waterbodies or other natural emissions. These previous sources are not included in the EDGAR inventory, but they could be detected by the RTM. However, those sources would not be able to fully explain the

sudden onset of increased RTM-based CH₄ fluxes but would rather contribute to a slow increase in warmer months. Further research applying isotopic analysis of CH₄ mixing ratios measured at the GIC3
695 station for the different seasons should be carried out, as well as transects of the regions to assess the impact of natural sources on CH₄ mixing ratios. In addition, no precise data on transhumant activity in Spain is available to date, but our study suggests the existence of a link between regional CH₄ fluxes and highlights the need for more information of transhumance activity which could be taken into account in future emission inventories of this region (and Europe). In addition, our results show that urban emissions
700 can be transported and could influence the atmospheric composition of remote rural areas over several hundred kilometres under specific synoptic conditions.

Acknowledgements

705

The research leading to these results has received funding from "la Caixa" Foundation with the ClimaDat project (2010-2014) and from the Ministerio Español de Economía y Competividad, Retos 2013 (2014-2016) with the MIP (Methane interchange between soil and air over the Iberian Península) project (reference: CGL2013-46186-R). This study was also made possible thanks to collaboration with the
710 Autonomous Community of Castile and León and the Sierra de Gredos Regional Park.

C. G. particularly thanks the Ministerio Español de Educación, Cultura y Deporte for partially supporting her work with the research mobility grant "José Castillejos" (ref. CAs15/00042). The research of F.R.V. Has been funded and supported by the Chaire industrielle BridGES, a joint research program between
715 ThalesAleniaSpace, Veolia and the parent institutions of LSCE (CEA, CNRS, UVSQ).

The authors warmly thank: i) the LAO (Atmosphere and Ocean laboratory) team, in the persons of: Rosa Arias, Manel Nofuentes, Oscar Batet, Lidia Cañas, Silvia Borrás, Paola Occhipinti and Eusebi Vazquez, for their efforts in the installation, maintenance and calibration of all IC3 climatic stations and data,
720 including the GIC3 station, where this study has been performed; ii) the INTE team, in the persons of: Vicente Blasco and Juan Antonio Romero, for their work in the building of the ARMON installed at the GIC3 station; iii) Albert Jornet, software engineer of the IC3 who developed, together with Roger Curcoll, an automatic system for the daily running of FLEXPART backward simulations; iv) Dr. Israel López-Coto and the University of Huelva for the radon flux modelled data; v) Dr. Stefano Galmarini for
725 helping to improve the manuscript; vi) David Carslaw and Karl Ropkins, developers of the R package OpenAir (www.openair-project.org), used in the present work for data analysis; vi) the two anonymous reviewers for their comments and suggestions for improving our work.